Phytochemistry 147 (2018) 184–193

Contents lists available at ScienceDirect

Phytochemistry

journal homepage: www.elsevier.com/locate/phytochem

Isolation, purification, structural characterization and immunostimulatory activity of water-soluble polysaccharides from *Lepidium meyenii*

Zhengqi Zha [a, 1], Su-Yan Wang [a, 1], Weihua Chu [a], Yang Lv [a], Hongjin Kan [a], Qiuli Chen [b], Lili Zhong [a], Long Yue [c], Jinna Xiao [a], Ying Wang [a, *], Hongping Yin [a, **]

[a] School of Life Science and Technology, State Key Laboratory of Natural Medicines, China Pharmaceutical University, Nanjing 210009, People's Republic of China
[b] School of Pharmacy, Nanjing University of Chinese Medicine, Nanjing 210029, People's Republic of China
[c] School of Engineering, China Pharmaceutical University, Nanjing 210009, People's Republic of China

ARTICLE INFO

Article history:
Received 12 September 2017
Received in revised form
5 January 2018
Accepted 7 January 2018

Keywords:
Lepidium meyenii Walp
Polysaccharide
Macrophage RAW264.7
Toll-like receptor (TLR)
Nuclear factor-κB

ABSTRACT

A water-soluble polysaccharide LMP-1 was isolated and purified by ion-exchange chromatography from maca (*Lepidium meyenii* Walp.). LMP-1 has a molecular weight of 1.01×10^4 Da, and is composed of glucose and arabinose with a molar ratio of 7.03:1.08. Methylation and the 1D and 2D NMR spectroscopy of LMP-1 revealed that it is mainly composed of →4)-α-D-Glc*p*-(1→, →6)-α-D-Glc*p*-(1→, →3)-α-D-Glc*p*-(1→, and β-D-Ara*f*-(1→, with branching at O-6 of →4,6)-α-D-Glc*p*-(1 → . LMP-1 showed up-regulation of Toll-like receptor 4 (TLR4) and Toll-like receptor 2 (TLR2). The upstream proteins of Toll-like receptors (TLRs) (CD14 and MD2) and mRNA level of IL-1β also increased. Increased transcription factor nuclear factor-kappa B (NF-κB) p65 was found in the nuclei and cytoplasm in LMP-1-treated RAW264.7 macrophages. These results indicated that LMP-1 activated RAW264.7 macrophages and elicited immunostimulatory activities via the TLRs/NF-κB signalling pathway.

1. Introduction

The immune system comprises many biological structures, such as tissues, cells, and molecules, and mediates resistance to infections (Hooper et al., 2012). Immune response can be classified into innate immunity and adaptive immunity in higher animals (Sun et al., 2015). Innate immunity is highly associated with macrophages, monocytes, granulocytes and humoural elements. Macrophages are important target cells when treated with immunomodulatory drugs (Chavez-Sanchez et al., 2014; Ma et al., 2011; Sun et al., 2015; Wang et al., 2016). In fact, activation of macrophages is now considered a promising strategy to improve host immune capability (Ma et al., 2011).

Toll-like receptors (TLRs) are known to play a critical role in early innate immune response. Among 13 members of the mammalian TLR family, TLR4 is responsible for recognition of lipopolysaccharide (LPS). Furthermore, TLR4 is the only TLR that mediates signal transduction through both myeloid differentiation factor 88 (MyD88) and Toll/IL-1 receptor-domain-containing adapter-inducing interferon-β- (TRIF-) mediated signalling pathways. An additional co-receptor, myeloid differentiation factor-2 (MD-2), is required to form a TLR4/MD-2 complex to regulate the recognition of LPS. The TLR4/MD-2 complex on host cell membranes recognizes LPS, with MD-2 directly binding to the lipid A moiety of LPS. Extracellular component CD14 is required for activation of the TRIF-dependent pathway (Jiang et al., 2005). CD14 also extends TLR4 recognition of LPS, followed by activation of downstream factors such as MyD88 and TRIF, which subsequently elevate NF-κB both in the cytoplasm and the nucleus (Akashi et al., 2000). Eventually, the increased dissociation of the NF-κB p65 subunit improves the transcription of TNF-α, interleukin (IL)-1β and IL-6 cytokines, thus activating the immune system (Hajjar et al., 2012).

* Corresponding author. No. 24 Tongjiaxiang Road, Nanjing 210009, Jiangsu, People's Republic of China.
** Corresponding author. No. 24 Tongjiaxiang Road, Nanjing 210009, Jiangsu, People's Republic of China.
E-mail addresses: ywang@cpu.edu.cn (Y. Wang), yinhongping63@hotmail.com (H. Yin).
[1] Both the authors worked equally to this work.

https://doi.org/10.1016/j.phytochem.2018.01.006
0031-9422/

Naturally derived polysaccharides were reported to possess immunomodulatory activity via macrophage activation via multiple routes, as well as anti-inflammation, anti-oxidation, and anti-tumour activity (Wu et al., 2014). Botanical polysaccharides are considered ideal immunomodulators due to their lower toxicity and lower side effects compared to insect and bacterial polysaccharides (Petrovsky and Cooper, 2011; Xiao et al., 2012; Sheu et al., 2013). Furthermore, botanical polysaccharides were revealed to enhance the immune effect in vaccines as excellent adjuvants (Sun et al., 2015; Licciardi and Underwood, 2011). *Lepidium meyenii* (*L. meyenii*) Walp, known as maca, is an annual or biennial herbaceous plant of the Brassicaceae family, which is cultivated mainly in the central Andes of Peru at an elevation of 3500–4500 m above sea level (Wang et al., 2007). The biological activities of maca include improving sexual function, regulating the endocrine system, and anti-fatigue and anti-oxidation activities. Few papers have been published about purified *L. meyenii* polysaccharides, despite much work focused on the glucosinolates, alkaloids and sterols of maca. Wang *et* al. reported that *L. meyenii* polysaccharide MP21, composed of rhamnose, arabinose and galactose, showed immunomodulatory effects by activating RAW264.7 via the NF-κB signalling pathway (Wang et al., 2016). *L. meyenii* polysaccharide LMP-60 possesses a good capability for scavenging hydroxyl free radical and superoxide radical at a concentration of 2.0 mg/mL (Zha et al., 2014). Another maca polysaccharide, MC-1 can significantly enhance pinocytic and phagocytic capacity and promote NO, TNF-α and IL-6 secretion in RAW 264.7 cells (Zhang et al., 2016). However, the exact structure and functional mechanism of MC-1 are unknown (Zhang et al., 2016).

In this study, a previously undescribed maca (*L. meyenii*) polysaccharide, LMP-1, was isolated, purified and clarified. The immunomodulatory activity mechanism of LMP-1 towards RAW264.7 macrophages was also studied.

2. Results and discussion

2.1. Isolation, purification, molecular weight and monosaccharide composition of LMP-1

Genome sequence results showed that the purchased root shared 97% similarity with maca, indicating that it was the same material. The purity of the crude *L. meyenii* polysaccharide (cLMP) was analysed using the anthrone-sulfuric acid method and was determined to be 66.7%. The protein content in cLMP was determined by the Bradford method as 5.4%. There was no uronic acid in cLMP. LMP-1 was collected from fractions using anion-exchange chromatography and a Sephadex G-100 column. The total sugar content of LMP-1 was determined as 99.8% using the anthrone-sulfuric acid method. No nucleic acid was present in LMP-1 (Data not shown). The molecular weight of LMP-1 was determined by high-performance gel permeation chromatography (HPGPC) using the Dextran T-series calibrated as a standard. The single symmetrical peak in Fig. 1A indicates that LMP-1 was a homogeneous polysaccharide. The apparent molecular weight of LMP-1 was 1.01×10^4 Da (Fig. 1B and C). The polydispersity index (Mw/Mn) of LMP-1 was 1.61. In addition, the monosaccharide composition of LMP-1 was determined using high-performance liquid chromatography (HPLC) to be glucose and arabinose in a molar ratio of 7.03:1.08 (Supplementary data 1). This is inconsistent with Wang's result, namely, that MP21 was mainly composed of rhamnose, arabinose and galactose in a molar ratio of 1:4.84:5.34 (Wang et al., 2016).

2.2. FT-IR spectroscopy analysis of LMP-1

The FT-IR spectrum of LMP-1 exhibited typical signals for polysaccharides in the range 4000 cm^{-1} to 400 cm^{-1}, and the characteristic absorption peak was apparent (Fig. 2). A strong and broad absorption peak of 3462.23 and 3143.47 cm^{-1} represent the stretching vibration of intramolecular hydrogen bonds and intermolecular hydrogen bonds, respectively (Cai et al., 2013). The band at 1634.90 cm^{-1} is attributed to the characteristic peak of bound water. Strong absorption peaks for pyranoside were at 1147.38, 1072.21 and 1018.52 cm^{-1}, representing two stretching vibrations of the C-O band and indicating the presence of a C-O-H bond and C-O-C bond. Peaks at 896.11, 859.60 and 831.68 cm^{-1} may be the resonance absorption peaks of pyranoside, with both α and β configurations (Cai et al., 2013).

2.3. Methylation and GC-MS analysis of LMP-1

Methylation and GC-MS analysis were performed to reveal the integrated structure of LMP-1 (Supplementary data 2). We identified peaks of partially methylated alditol acetates (PMAAs) by retention time in the GC by referring to mass spectra patterns in the literature (Carpita and Shea, 1989). Based on analysis of PMAAs, the linkages of LMP-1 are shown in Table 1. The results showed that the major alditol acetate derivatives from the methylated products of LMP-1 were 2,3,5-Me_3-Ara*f*, 2,3,4,6-Me_4-Glc*p*, 2,4,6-Me_3-Glc*p*, 2,3,6-Me_3-Glc*p*, 2,3,4-Me_3-Glc*p*, and 2,3-Me_2-Glc*p* at percentages of 6.31%, 13.25%, 7.09%, 53.66%, 6.24% and 13.45%, respectively. The presence of 1,4,6-linked-Glc*p* indicated that LMP-1 a contained branched structure. The presence of 2,3,6-Me_3-Glc*p* illustrated that the main composition was 1,4-linked-glucose, and 2,3,5-Me_3-Ara*p* illustrated the presence of 1-linked-arabinose at the end of the main chain or branched chain.

2.4. Analysis of nuclear magnetic resonance (NMR)

Based on the NMR analysis, the main chemical shifts for LMP-1 were found and presented in Table 2. ^{1}H NMR (Fig. 3A) and ^{13}C NMR (Fig. 3B) spectra were crowded from δ 3.0–5.5 ppm (^{1}H NMR) and δ 60–110 ppm (^{13}C NMR), respectively, in accordance with typical polysaccharides (Dang et al., 2013; Li et al., 2013). Anomeric proton signals at δ 4.81, 5.07, 5.00, 5.20, 5.24, and 5.03 ppm, and anomeric carbon signals at δ 109.99, 99.56, 99.70, 100.02, 99.87, and 99.48 ppm, revealed that LMP-1 might contain six types of monosaccharide residues. According to ^{1}H-^{1}H COSY (Fig. 3C) and HSQC (Fig. 3D) spectra (Nie et al., 2011), the anomeric proton and carbon signals were analysed as follows. Signals at δ 4.81/109.99, 5.07/99.56, 5.00/99.70, 5.20/100.02, 5.24/99.87 and 5.03/99.48 ppm were assigned to the H-1/C-1 of β-D-Ara*f*-(1→, α-D-Glc*p*-(1→, →3)-α-D-Glc*p*-(1→, →4)-α-D-Glc*p*-(1→, →6)-α-D-Glc*p*-(1→, →4,6)-α-D-Glc*p*-(1→ residues, respectively (Shakhmatov et al., 2017; Xu et al., 2015; Pan et al., 2015a,b). Signals at δ 73.40, 73.25, 71.48, 69.24 and 66.10 ppm corresponded through C-2-C-6 of →6)-α-D-Glc*p*-(1→ (He et al., 2017). Signals at δ 73.40, 73.25, 76.85, 69.24 and 66.10 ppm were attributed to C-2-C-6 of →4,6)-α-D-Glc*p*-(1→ respectively (Xu et al., 2015). Signals at δ 73.40, 73.25, 76.99, 69.24, and 60.40 ppm were attributed to the C-2-C-6 of →4)-α-D-Glc*p*-(1→. Signals at δ 73.40, 76.61, 70.29, 69.24, and 60.40 ppm were attributed to the C-2-C-6 of →3)-α-D-Glc*p*-(1→ (Ma et al., 2014). Signals at δ 73.40, 73.25, 70.29, 69.24, and 60.40 ppm were attributed to C-2-C-6 of α-D-Glc*p*-(1→ (Xu et al., 2015). Signals at δ 72.90, 69.24, 71.24, and 60.59 ppm were attributed to C-2-C-6 of β-D-Ara*f*-(1→ (Shakhmatov et al., 2017).

To further evaluate the structural information, the HMBC spectra were analysed (Fig. 3E). The results demonstrated

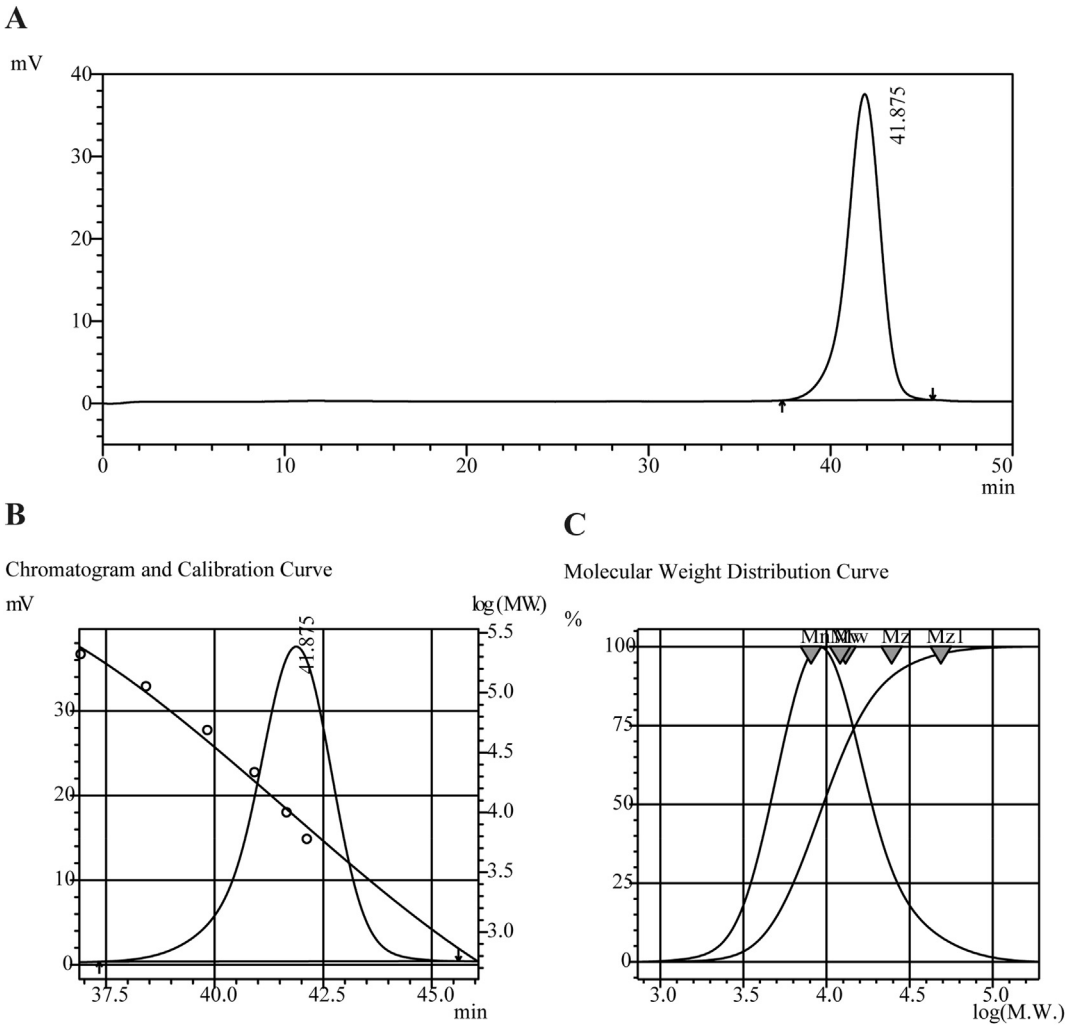

Fig. 1. Elution profile of LMP-1 in HPGPC with 0.1 M $NaNO_3$ at a flow rate of 0.35 mL/min on Shodex SB805 and 802 columns. (A) LMP-1 was identified as a single symmetrical sharp peak, indicating a homogeneous polysaccharide. (B) Weight-averaged molecular weight (Mw) of LMP-1. (C) Chromatogram and calibration curve of Dextran standards plotted with GPC software and Mw on a log scale versus the retention time.

correlations from the H-1 (*δ* 5.24 ppm) of →6)-α-D-Glc*p*-(1→ residue to the C-4 (*δ* 76.85 ppm) of →4,6)-α-D-Glc*p*-(1→ residue (Shi et al., 2012). In addition, correlations from H-1 (*δ* 5.20 ppm) of →4)-α-D-Glc*p*-(1→ residue to C-4 (*δ* 76.99 ppm) of →4)-α-D-Glc*p*-(1→ residue (Pau-Roblot et al., 2013), and from H-6 (*δ* 3.79 ppm) of →4,6)-α-D-Glc*p*-(1→ residue to C-3 (*δ* 76.61 ppm) of →3)-α-D-Glc*p*-(1→ residue were revealed, respectively (Pu et al., 2016). The H-4 (*δ* 3.45 ppm) signal of →4)-α-D-Glc*p*-(1→ correlated with the C-1 (*δ* 99.48 ppm) of →4,6)-α-D-Glc*p*-(1→ residue (Shang et al., 2012), from the H-1 (δ 5.07 ppm) of α-D-Glc*p*-(1→ residue to the C-1 (δ 99.70 ppm) of →3)-α-D-Glcp-(1→ residue (Li et al., 2017; Pan et al., 2015a,b), and from the H-1 (δ 4.81 ppm) of β-D-Ara*f*-(1→ residue to the C-6 (δ 69.24 ppm) of →6)-α-D-Glc*p*-(1→ residue (Xia et al., 2015), respectively.

Comprehensive analysis of methylation, monosaccharide composition, FT-IR spectroscopy and NMR data revealed a prediction about the primary structure of LMP-1, as shown in Fig. 4.

2.5. Effects of LMP-1 on cell viability of RAW264.7

The 3-(4,5-dimethyl-2-thiazolyl)-2,5-diphenyl-2-H-tetrazolium bromide (MTT) assay was used to determine the proliferation and cytotoxicity of LMP-1 towards RAW264.7 cells. LPS showed promoted proliferation of RAW264.7 cells, and no obvious cytotoxicity was found in LPS-treated cells compared to a blank control (Supplementary data 3A). A 1 μg/mL LPS sample was selected as a positive control, and the results showed that 1.56–12.5 μg/mL LMP-1 could significantly promote the proliferation of macrophages when incubated for 24 h (Supplementary data. 3B). Therefore, 1.56 μg/mL, 3.125 μg/mL and 6.25 μg/mL of LMP-1 were selected to treat RAW264.7 macrophages in further studies.

2.6. LMP-1 regulated protein expression of TLRs and its upstream proteins in RAW264.7 cells

TLRs recognize a variety of pathogenic structures, thus playing a central role in the innate immune response (Manček-Keber and Jerala, 2015). The TLR4 signalling pathway can be initiated in LPS-activated macrophages. TLR4 specifically recognizes LPS by binding to its co-receptor MD-2. This leads to the activation of NF-κB, which induces expression of proinflammatory cytokines including TNF-α, IL-1β, and IL-6, (Li and Xu, 2011). CD14, an exterior receptor of LPS, can assist LPS in the recognition of TLR4 and transfer the complex to MD-2 (Akashi et al., 2000). CD14 is also required for activation of the TRIF-dependent pathway (Jiang et al., 2005), and a Western blot was used to detect TLRs, CD14 and MD2. Elevated

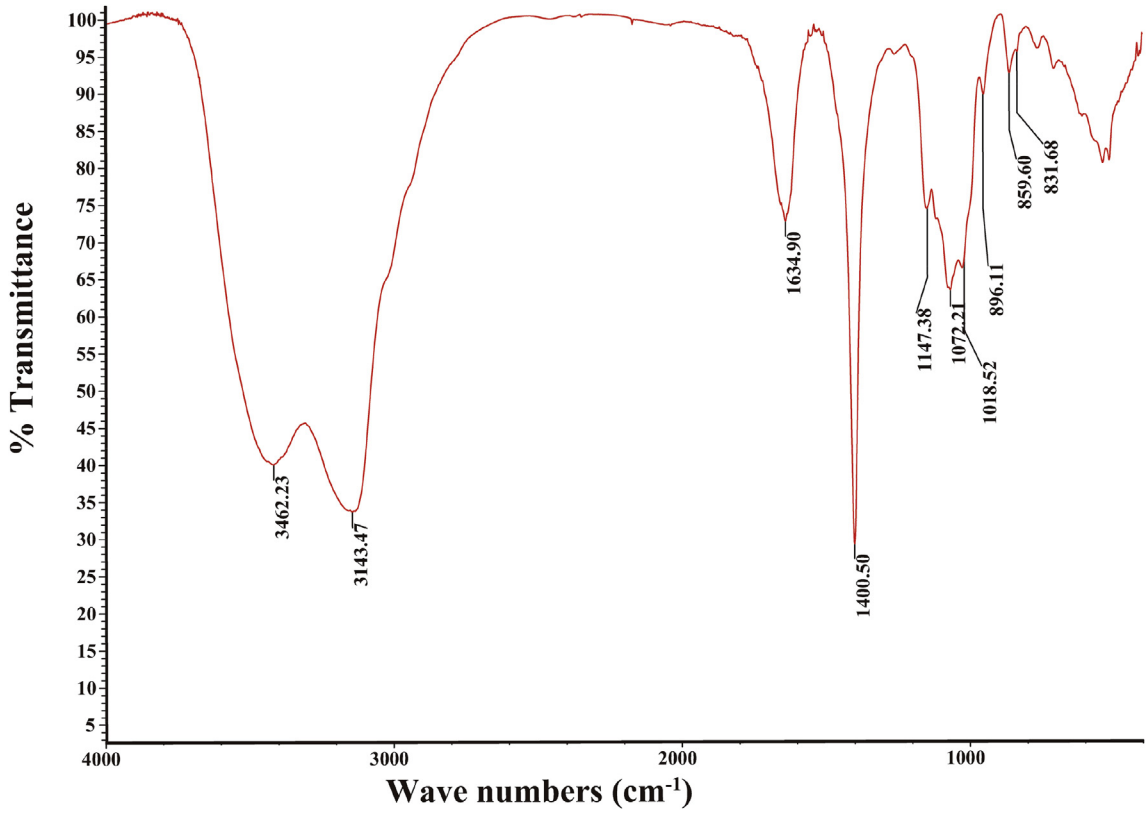

Fig. 2. Spectrum of FT-IR of LMP-1.

Table 1
GC-MS of main alditol acetate derivatives from the methylated products of LMP-1.

Methylated sugars (as alditol acetates)	Type of linkage	Percentage of linkage (%)	Mass fragments (m/z) (Relative abundance, %)
2,3,5-Me_3-Ara*f*	T-Ara*f*	6.31	43,45,71,87,101,117,129,145,161
2,3,4,6-Me_4-Glc*p*[a]	T-Glc*p*	13.25	43,45,59,71,87,101,117,129,145,161,205
2,4,6-Me_3-Glc*p*	1,3-linked-Glc*p*	7.09	43,45,71,87,101,117,129,161,233
2,3,6-Me_3-Glc*p*	1,4-linked-Glc*p*	53.66	43,45,71,87,99,113,117,129,161,233
2,3,4-Me_3-Glc*p*	1,6-linked-Glc*p*	6.24	43,45,71,87,101,117,129,161,189,233
2,3-Me_2-Glc*p*	1,4,6-linked-Glc*p*	13.45	43,45,71,87,101,117,129,261

[a] 2,3,4,6-Me_4-Glc*p* = 1,5-di-*O*-acetyl-2,3,4,6-tetra-*O*-methyl-Glucopyranose, etc.

Table 2
^{13}C NMR and ^{1}H NMR chemical shifts of the main residues from LMP-1 in D_2O.

Sugar residue	$\delta^{13}C/^{1}H$ (ppm)					
	1	2	3	4	5	6
β-D-Ara*f*-(1→	109.99	72.90	69.24	71.24	60.59	–
	4.81	3.55	3.26	3.68	3.59/3.65	–
α-D-Glc*p*-(1→	99.56	73.40	73.25	70.29	66.10	60.40
	5.07	3.87	3.81	3.55	3.28	3.49/3.69
→3)-α-D-Glc*p*-(1→	99.70	73.40	76.61	70.29	66.10	60.40
	5.00	3.87	3.79	3.55	3.28	3.49/3.69
→4)-α-D-Glc*p*-(1→	100.02	73.40	73.25	76.99	66.10	60.40
	5.20	3.87	3.81	3.45	3.28	3.49/3.69
→6)-α-D-Glc*p*-(1→	99.87	73.40	73.25	71.48	66.10	69.24
	5.24	3.87	3.81	3.45	3.28	3.66/3.79
→4,6)-α-D-Glc*p*-(1→	99.48	73.40	73.25	76.85	66.10	69.24
	5.03	3.87	3.81	3.79	3.26	3.66/3.79

levels of TLR4 and TLR2 were noticed in the middle-dose (3.125 μg/mL) and high-dose (6.25 μg/mL) LMP-1-treated RAW264.7 cells compared to the control group, using β-actin as standard (Fig. 5A). Both 1 μg/mL LPS and 6.25 μg/mL lentinan (LNT) showed similar effects on the enhanced expression of TLR4 and TLR2. We speculated that LMP-1 possesses similar effects compared to LPS in activating macrophages. Thus, we further detected the up-stream proteins of TLRs. An obvious increase in MD2 was noticed in LMP-1-, LPS- and LNT-treated RAW264.7 cells compared to the control group (Fig. 5A). A distinct improvement in CD14 expression was noticed only in high-dose LMP-1-treated cells. Hence, we infer that LMP-1 binds to CD14 and MD2 to form a complex, thus extending to TLRs and activating macrophages.

2.7. LMP-1 induced expression of inflammatory factors in macrophages

To determine the immunostimulatory activity of LMP-1, the mRNA levels of inflammatory cytokines were measured. TNF-α is mainly produced by activated macrophage, which plays a critical role in regulating immune cells towards inflammatory response (Ji et al., 2015). IL-1β and IL-6 also actively participate in macrophage-associated immune responses (Sun et al., 2015). The mRNA level of TNF-α, IL-1β and IL-6 increased in LMP-1-treated RAW264.7 cells in a dose-dependent manner compared to the control (Fig. 5B),

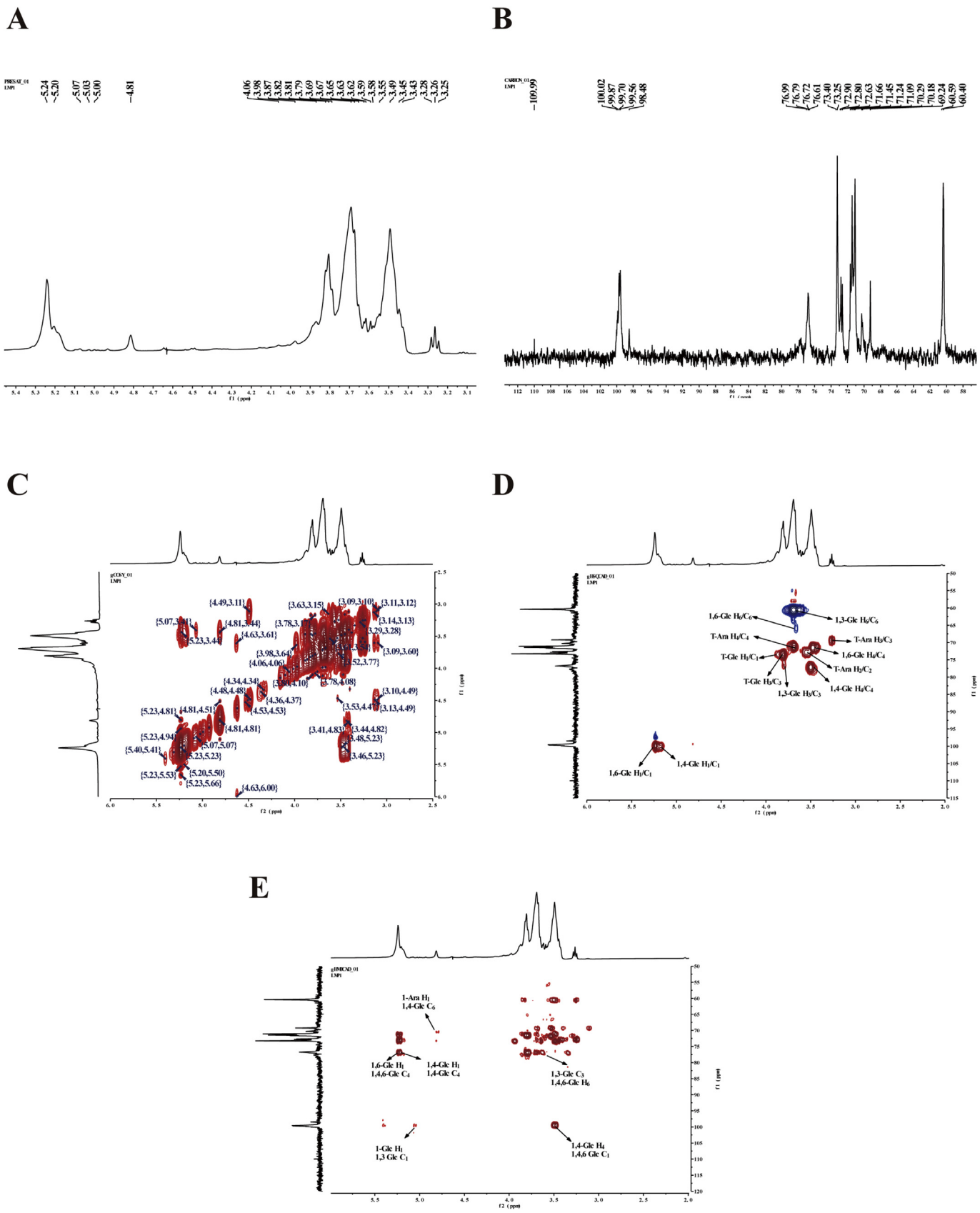

Fig. 3. NMR spectra of LMP-1. (A) ^{1}H NMR spectrum. (B) ^{13}C NMR spectrum. (C) ^{1}H-^{1}H COSY spectrum. (D) HSQC spectrum. (E) HMBC spectrum in D_2O.

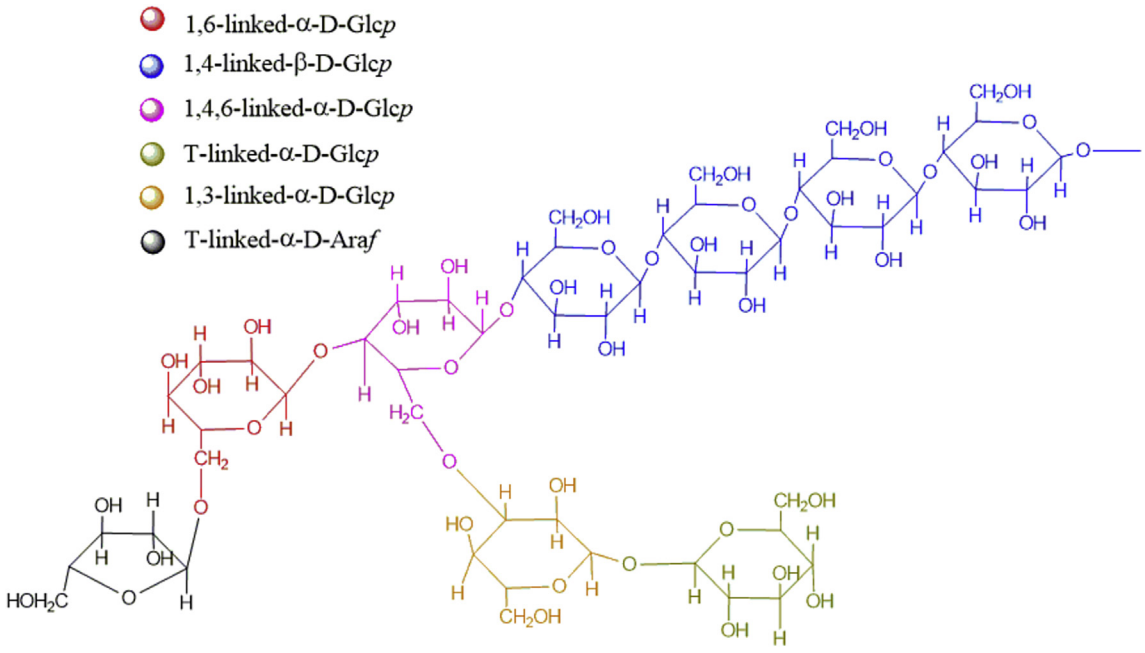

Fig. 4. Predicted structure of LMP-1.

indicating the immunostimulatory activity of LMP-1. Enhanced mRNA levels of TNF-α, IL-1β and IL-6 were also observed in LPS-treated cells. LNT, however, induced less mRNA in cytokines compared to the concentration of LMP-1 (Fig. 5B). Real-time quantitative PCR demonstrated that LMP-1 can induce inflammatory cytokines by activating macrophages.

2.8. LMP-1 induced mRNA level of MyD88, TRIF, TRAF3, TRAF6 and TBK1 in RAW264.7 cells

Recognition of microbial components (e.g., LPS, lipoprotein, flagellin and nucleic acids) by TLR-initiated inflammatory signal cascades via two distinct pathways: (i) the MyD88-dependent pathway and (ii) the TRIF-dependent pathway (Vallabhapurapu et al., 2008). MyD88 is an adapter molecule that triggers inflammatory signals commonly utilized by various TLRs distinct from TLR3. IκB kinase (IKK) and TANK-binding kinase 1 (TBK1) participate in regulating the interferon regulatory factor (IRF) and NF-κB signal pathways by forming a heterogeneous dimer (Takeda and Akira, 2005; Lee et al., 2010). Tumour necrosis factor receptor-associated factor (TRAF) family proteins are frequently involved in the downstream signalling pathway of TLRs to evoke immune responses (Wu et al., 2010). In the TRAF family, TRAF6 and TRAF3 are important in signal transduction associated with TLR superfamilies (Aderem and Ulevitch, 2000), and the mRNA level of TRIF and MyD88 were strengthened in the middle-dose and high-dose LMP-1-treated RAW264.7 cells compared to the control group (Fig. 5C). Similar mRNA levels were observed in LPS compared to high-dose LMP-1. LNT exhibited the highest mRNA level of MyD88 and constant mRNA level of TRIF (Fig. 5C). The heightened mRNA level of TRAF3 and TRAF6 were observed in middle-dose and high-dose LMP-1-treated RAW264.7 cells, as well as for LPS compared to the control group (Fig. 5D). An increased mRNA level of TRAF3 was determined in LNT-treated cells but there was no increase in TRAF6 (Fig. 5D). The results revealed that LMP-1 could act through both the MyD88 and TRIF-dependent TLR signal pathways.

2.9. LMP-1 activates NF-κB signalling pathway in macrophages

TBK1 is a serine/threonine protein-kinase-mediating innate antimicrobial immunity (Shu et al., 2013.). TBK1 is involved in signalling of TLRs, RLRs and is a stimulator of interferon genes (STING)-mediated sensing of cytosolic DNA (Helgason et al., 2013.). Stimulation of TLRs and RLRs results in TBK1 activation, and hence phosphorylating interferon regulatory factor (IRF)-3. Phosphorylated IRF-3 can be translocated into the nucleus, leading to transcription initiation of TNF-α and proinflammatory genes such as IL-6 and IL-1β (Abe and Barber, 2014). NF-κB can be translocated from the cytoplasm to nucleus, where it regulates transcription of proinflammatory cytokines such as TNF-α, IL-1β and IL-6. According to Fig. 5E, the mRNA level of TBK1 significantly increased in LMP-1-treated RAW264.7 cells. In addition, LMP-1 promoted the mRNA level of NF-κB in a concentration-dependent manner. LNT had auxo-action only on mRNA level of TBK1 (Fig. 5E). NF-κB is an important immunoregulation factor that acts in infection response by up-regulating cytokine gene transcription. (Ma et al., 2011). Therefore, we examined the effect of LMP-1 on NF-κB p65 expression in the nucleus and cytoplasm of RAW264.7 cells. As shown in Fig. 5F, LMP-1 elevated the NF-κB p65 level in the nucleus in dose-dependent manner using β-actin as standard, consistent with the results in the cytoplasm. A higher concentration of NF-κB p65 was noticed in the nucleus that in the cytoplasm. Therefore, LMP-1 promoted translocation of NF-κB p65 from the cytoplasm into the nucleus, thus activating transcription of cytokine genes.

3. Materials and methods

3.1. Materials

The dried roots of maca (*Lepidium meyenii* Walp.), were verified using DNA sequencing technology. Maca was purchased from Jiangsu Biomedical Technology Co., Ltd., and the company conducted preliminary processing of maca from Jade Dragon Snow Mountain in Lijiang, Yunnan Province, China (100°4′2″E, 27°3′2″N). The genome fragments of maca roots were amplified and compared

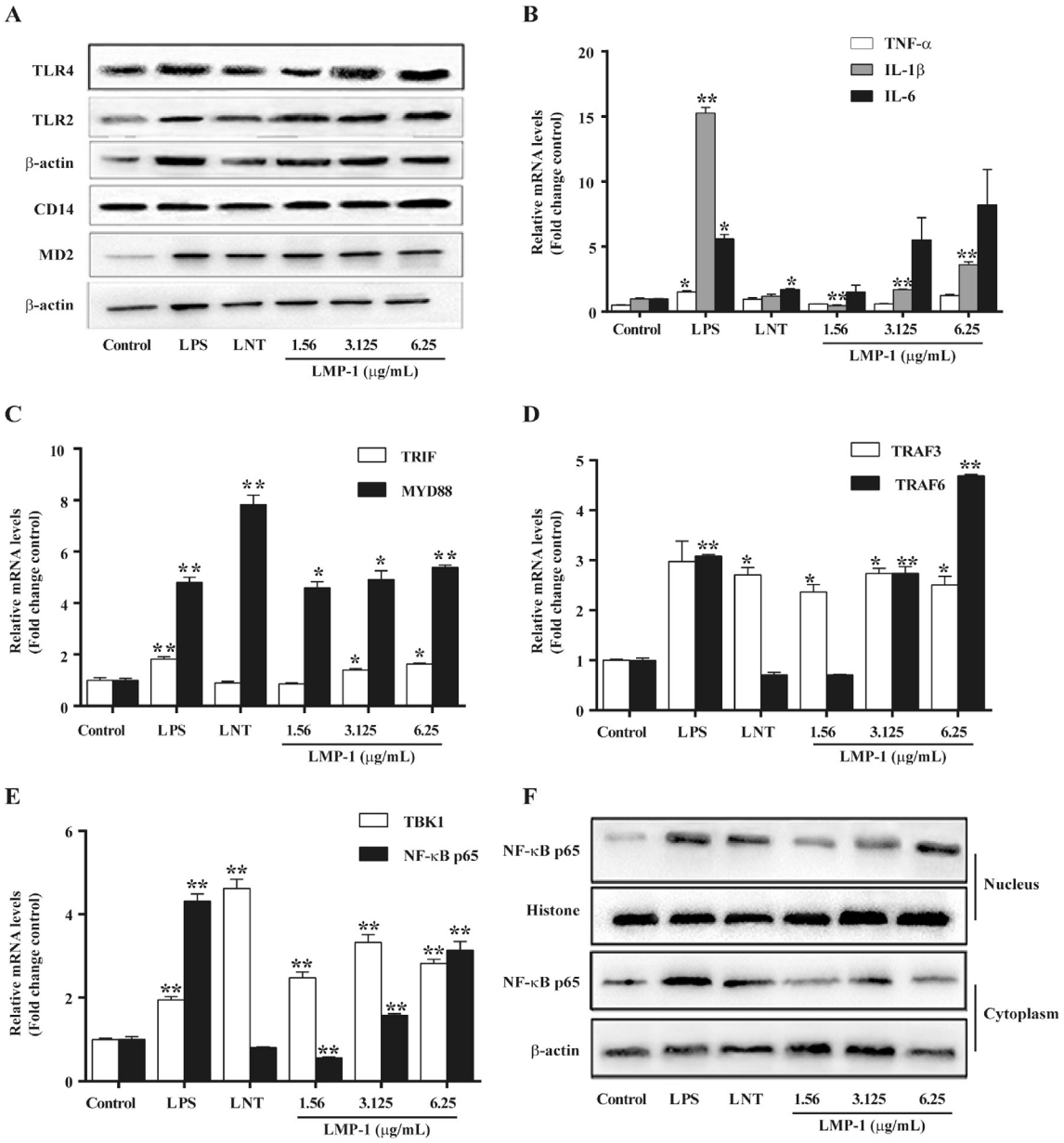

Fig. 5. LMP-1 regulated mRNA and protein expression of TLRs and upstream/downstream genes in RAW264.7 cell. (A) Protein expression levels of TLR4, TLR2, MD2 and CD14, standardized by β-actin. (B) mRNA expression of TNF-α, IL-1β, and IL-6 measured. (C) mRNA expression of TRIF and MyD88. (D) mRNA expression of TRAF3 and TRAF6. (E) mRNA expression of TBK1 and NF-κB p65 in RAW264.7. (F) Protein expression of nuclear NF-κB p65 and cytoplasmic NF-κB p65. Data were expressed as the means ± SD, n = 3. $^{*}p < .05$, $^{**}p < .01$ vs control.

to the genome of *L. meyenii* Walp reported in NCBI.

DEAE-cellulose, Sephadex G-100, TFA and PMP and MTT were purchased from Amersham Biosciences (USA). All other chemicals and solvents were analytical reagent grade. Lipopolysaccharides (LPS, from *Escherichia coli* O55: B5, L2880), dextran and nine monosaccharides including mannose, ribose, rhamnose, glucuronic acid, galacturonic acid, glucose, galactose, arabinose, and fucose were obtained from Sigma-Aldrich (Shanghai, China). Lentinan (LNT) was obtained from the Nanjing Kang Hai Pharmaceutical Co., Ltd. (Nanjing, China). Dulbecco's modified Eagle medium (DMEM) was purchased from WISENT (Nanjing, China). Foetal bovine serum (FBS) was obtained from Biological Industries (Israel). TRIzol was obtained from Invitrogen (USA). Rabbit polyclonal antibodies against β-actin (D110001-0100) were obtained from Life Sciences (USA). Rabbit anti-mouse CD14 polyclonal antibodies (BA0719-2) and NF-κB p65 (Ser536) monoclonal antibody (BA061078611P114) were purchased from Boster, Inc. (Wuhan, China). Monoclonal antibodies against TLR4 (19811-1-AP) and TLR2 (17236-1-AP) were purchased from Proteintech (Wuhan, China).

3.2. Extraction and purification of *L. meyenii* polysaccharide

The rhizome of *L. meyenii* (100 g) was smashed and stirred twice in 2000 mL water at 95 °C. The aqueous extract was condensed with a rotary evaporator under vacuum and the concentrated solution was precipitated with 95% ethanol to a final concentration of 80%. After centrifuging at 5000 rpm for 10 min, the precipitate was collected and dissolved in distilled water before precipitation with 95% ethanol. The resultant precipitate was collected and washed with anhydrous ethanol twice to obtain the crude polysaccharides

(marked as cLMP, 5.3371 g). The cLMP was dissolved in distilled water and adjusted to pH 2.0 for 24 h. The solution was dialyzed and lyophilized before application to a DEAE (Cl^-)-cellulose (8 × 25 cm) column (Supplementary data 4A). The main ingredient was eluted with distilled water, collected and lyophilized for further purification. The lyophilized powder was dissolved in water before loading onto Sephadex G-100 (1 × 80 cm) column and eluted with distilled water to obtain the major fraction, named LMP-1 (Supplementary data 4B). The Bradford (Compton and Jones, 1985) assay and UV absorbance at 260 nm and 280 nm were conducted to determine the protein and nucleotide impurity of LMP-1.

3.3. Apparent molecular weight

HPGPC was used to determine the homogeneity and molecular weight of LMP-1; briefly, a 2 mg/mL sample was loaded onto a Waters HPLC equipped with Shodex OHpak SB-805 and an 802 tandem chromatographic column (7.8 mm × 300 mm) with 0.1 M $NaNO_3$ as the eluent at a flow rate of 0.35 mL/min. The column was calibrated with Dextran standards of different molecular weights. The apparent molecular weight of LMP-1 was estimated with the standard curve prepared above.

3.4. Monosaccharide composition analysis

HPLC analysis was performed to determine the monosaccharide composition and molar ratio by 3-Methyl-1-Phenyl-5-pyrazolone (PMP) labelling (Dai et al., 2010). Briefly, 5 mg/mL LMP-1 (1 mL) was mixed with the same volume of 2 M trifluoroacetic acid (TFA). The resulting solution was incubated at 100 °C for 2 h, followed by co-distillation with methanol. The resulting mixture was dissolved in distilled water and derived with 0.4 M PMP solution (dissolved in 0.6 M NaOH) at 60 °C for 100 min. The solution was subsequently neutralized with 0.3 M HCl and extracted with 1 mL chloroform three times. Then, 10 μL of the aqueous phase was loaded onto a ZORBAX Eclipse XDB-C18 (250 mm × 4.6 mm) column with 1.0 mL/min constant elution containing acetonitrile and phosphate buffer (pH 6.7) in a ratio of 17: 83 (v/v). Various monosaccharides were processed as standards.

3.5. FT-IR spectroscopy

A 5-mg LMP-1 powder sample was mixed with KBr powder (spectroscopic grade) and pressed into a 1-mm pellet for FT-IR measurement. The FT-IR spectrum was determined using a Fourier transform infrared spectrophotometer (Bruker Tensor 27, Bruker, Germany) at a frequency range of 400–4000 cm^{-1}.

3.6. Methylation and GC-MS

A 5-mg LMP-1 sample was completely dissolved in dimethylsulfoxide under nitrogen protection according to the Ciucanu method (Ciucanu and Kerek, 1984). NaOH powder was added to the solution and stirred to dissolve at room temperature. Methyl iodide was added to the mixture dropwise, vortexed and stirred for 3 h. The organic phase was extracted three times using dichloromethane. The extract was dried under nitrogen. After three rounds of methylation, the residues were hydrolysed with 2 M TFA. One eq. of methanol and moderate ammonia were added to the above mixture to adjust the pH to 9.0. Sufficient $NaBH_4$ was added and the reaction was stirred at room temperature for 8 h. The resulting solution was acetylated with acetic anhydride at 100 °C for 2 h and dissolved in dichloromethane, which was subsequently loaded onto an Na_2SO_4 column and eluted with dichloromethane. PMAAs were analysed by gas chromatography-mass spectrometry (GC–MS) on an HP 6890II instrument using a DB-225MS fused-silica capillary column (Agilent Technologies Co. Ltd., USA).

3.7. NMR

A 40-mg LMP-1 sample was dissolved in 99.99% D_2O, and 1D (^1H and ^{13}C NMR) and 2D NMR, ^1H-^1H Correlated Spectroscopy (^1H-^1H COSY), Heteronuclear Singular Quantum Correlation (HSQC) and Heteronuclear Multiple Bond Correlation (HMBC) spectra were performed at 25 °C with a JEOL JNM-ECP 600 NMR spectrometer (JEOL, Tokyo, Japan). All chemical shifts referred to acetone-*d*6.

3.8. Biological activity in vitro

3.8.1. Cell viability assay

RAW264.7 macrophages were cultured in 5% CO_2 with DMEM medium containing 10% FBS and 1% penicillin/streptomycin at 37 °C for 24 h. The effect of LMP-1 on the viability of RAW264.7 cells was determined by the MTT method as follows: RAW264.7 cells were seeded at 3 × 10^4 cells/well in 96-well plates with different concentrations of LMP-1 (0, 0.39, 0.78, 1.56, 3.125, 6.25, 12.5 and 25 μg/mL) and incubated for 48 h. A 1 μg/mL LPS sample was used as a positive control. 20 μL of MTT (5 mg/mL) was added to each well and incubated for 4 h, and 150 μL dimethylsulfoxide was added to each well and shaken for 10 min. Data were collected at 570 nm using a microplate reader. All experiments were performed in triplicate.

3.8.2. Reverse transcription and real-time quantitative PCR

Total mRNA, isolated from RAW264.7, was treated with LMP-1 or LPS using the TRIzol Plus reagent following the manufacturer's instructions. Total cDNAs was reverse transcribed using Oligo dT 18 primer with the BU-SuperScript RT Kit (Biouniquer, China) in a total volume of 20 μL. The quantification of mRNA was determined using an ABI 7700 Prism Sequence Detection System and TaqMan primer probes (Applied Biosystems, USA). The results were expressed as the ratio of the optimal density to GAPDH. Primer sequences are listed in Supplementary data 5.

3.8.3. Western blot analysis

RAW264.7 cells were treated with LMP-1 for 30 min and washed twice with cold PBS. NE-PERTM nucleus and cytoplasmic extraction reagents were purchased from Pierce, USA. Protein extracts from the nucleus and cytoplasm were processed using kits supplied by Shanghai Biological Engineering Technology Service Co., Ltd. Denatured proteins were separated using 10–12% sodium dodecyl sulfate polyacrylamide gel electrophoresis (SDS-PAGE), and transferred to PVDF membranes. Anti NF-κB p65, TLR4, TLR2, CD14, MD2 and β-actin antibodies were used, and loaded proteins were normalized to β-actin. Signals were exposed to X-ray films using the ECL Detection Kit. The bands were visualized and photographed using JS-680B Gel Documentation and Analysis System. All experiments were performed in triplicate.

3.9. Statistical analysis

All data were expressed as the mean ± SD (standard deviation). All values were calculated using SPSS software. Statistical analysis of experimental data and controls were conducted using one-way analysis of variance (ANOVA) followed by Student-Newman-Keuls post hoc multiple comparison tests. $^*p < .05$ and $^{**}p < .01$ were considered statistically significant.

4. Conclusion

In conclusion, LMP-1, isolated from *L. meyenii*, was structurally characterized and was composed of glucose and arabinose in a molar ratio of 7.03:1.08 with a molecular weight of 1.01×10^4 Da. The main backbone consisted of →[1)-α-D-Glc*p*-(4]$_4$ → 1)-α-D-Glc*p*-(4 → 1)-α-D-Glc*p*-(6 → 1)-α-D-Ara*f*, and residues formed branches of →3)-α-D-Glc*p*-(1 → 1)-β-D-Glc*p* with the O-6 position of →1)-α-D-Glc*p*-(4,6 → . LMP-1 had significant effects on immunostimulatory activity in RAW264.7 macrophages through the TLRs/NF-κB pathway (supplementary data 6). The current study indicates that LMP-1 might be an effective drug candidate for immunoregulation and food additives for immunocompromised people.

Conflicts of interest

The authors confirm that there are no conflicts of interest.

Acknowledgements

This work was supported by the National Natural Science Foundation of China (No. 81773985), Industry-University-Institute Cooperation Project of Science & Technology Department of the Jiangsu provincial government (No.BY2015072-01), and the Fundamental Research Funds for the Central Universities (No.2016ZPY002). The project was funded by the Priority Academic Program Development of Jiangsu Higher Education Institutions (PAPD).

Appendix A. Supplementary data

Supplementary data related to this article can be found at https://doi.org/10.1016/j.phytochem.2018.01.006.

References

Abe, T., Barber, G.N., 2014. Cytosolic-DNA-mediated, STING-dependent proinflammatory gene induction necessitates canonical NF-kappa B activation through TBK1. J. Virol. 88, 5328–5341.
Aderem, A., Ulevitch, R.J., 2000. Toll-like receptors in the induction of the innate immune response. Nature 406, 782–787.
Akashi, S., Ogata, H., Kirikae, F., Kirikae, T., Kawasaki, K., Nishijima, M., Shimazu, R., Nagai, Y., Fukudome, K., Kimoto, M., Miyake, K., 2000. Regulatory roles for CD14 and phosphatidylinositol in the signaling via toll-like receptor 4-MD-2. Biochem Bioph Res Co 268, 172–177.
Cai, W.R., Xie, L.L., Chen, Y., Zhang, H., 2013. Purification, characterization and anticoagulant activity of the polysaccharides from green tea. Carbohydr. Polym. 92, 1086–1090.
Carpita, N.C., Shea, E.M., 1989. Linkage structure of carbohydrates by gas chromatography-mass spectrometry of partially methylated alditol acetates. https://www.researchgate.net/publication/303637085_Linkage_structure_of_carbohydrates_by_gas_chromatography-mass_spectrometry_of_partially_methylated_alditol_acetates.
Chavez-Sanchez, L., Espinosa-Luna, J.E., Chavez-Rueda, K., Legorreta-Haquet, M.V., Montoya-Diaz, E., Blanco-Favela, F., 2014. Innate immune system cells in atherosclerosis. Arch. Med. Res. 45, 1–14.
Ciucanu, I., Kerek, F., 1984. A simple and rapid method for the permethylation of carbohydrates. Carbohydr. Res. 131, 209–217.
Compton, S.J., Jones, C.G., 1985. Mechanism of dye response and interference in the Bradford protein assay. Anal. Biochem. 151, 369–374.
Dai, J., Wu, Y., Chen, S.W., Zhu, S., Yin, H.P., Wang, M., Tang, J.A., 2010. Sugar compositional determination of polysaccharides from Dunaliella salina by modified RP-HPLC method of precolumn derivatization with 1-phenyl-3-methyl-5-pyrazolone. Carbohydr. Polym. 82, 629–635.
Dang, Z.L., Feng, D.M., Liu, X.H., Yang, T., Guo, L., Liang, J., Liang, J.D., Hu, F.D., Cui, F., Feng, S.L., 2013. Structure and antioxidant activity study of sulfated acetamidopolysaccharide from Radix Hedysari. Fitoterapia 89, 20–32.
Hajjar, A.M., Ernst, R.K., Fortuno, E.S., Brasfield, A.S., Yam, C.S., Newlon, L.A., Kollmann, T.R., Miller, S.I., Wilson, C.B., 2012. Humanized TLR4/MD-2 mice reveal LPS recognition differentially impacts susceptibility to Yersinia pestis and Salmonella enterica. PLoS Pathog. 8 (10), e1002963.
He, P.F., He, L., Zhang, A.Q., Wang, X.L., Qu, L., Sun, P.L., 2017. Structure and chain conformation of a neutral polysaccharide from sclerotia of Polyporus umbellatus. Carbohydr. Polym. 155, 61–67.
Helgason, E., Phung, Q.T., Dueber, E.C., 2013. Recent insights into the complexity of Tank-binding kinase 1 signaling networks: the emerging role of cellular localization in the activation and substrate specificity of TBK1. FEBS Lett. 587, 1230–1237.
Hooper, L.V., Dan, R.L., Macpherson, A.J., 2012. Interactions between the microbiota and the immune system. Science 336, 1268.
Ji, G.Q., Chen, R.Q., Zheng, J.X., 2015. Macrophage activation by polysaccharides from Atractylodes macrocephala Koidz through the nuclear factor-κB pathway. Pharmaceut. Biol. 53, 512–517.
Jiang, Z., Georgel, P., Du, X., Shamel, L., Sovath, S., Mudd, S., Huber, M., Kalis, C., Keck, S., Galanos, C., 2005. CD14 is required for MyD88-independent LPS signaling. Nat. Immunol. 6, 565.
Lee, J.S., Kwon, J.S., Won, D.P., Lee, K.E., Shin, W.C., Hong, E.K., 2010. Study on macrophage activation and structural characteristics of purified polysaccharide from the liquid culture broth of Cordyceps militaris. Carbohydr. Polym. 82, 982–988.
Li, B., Dobruchowska, J.M., Gerwig, G.J., Dijkhuizen, L., Kamerling, J.P., 2013. Structural investigation of water-soluble polysaccharides extracted from the fruit bodies of Coprinus comatus. Carbohydr. Polym. 91, 314–321.
Li, X.Q., Xu, W., 2011. TLR4-mediated activation of macrophages by the polysaccharide fraction from Polyporus umbellatus(pers.) Fries. J. Ethnopharmacol. 135, 1–6.
Licciardi, P.V., Underwood, J.R., 2011. Plant-derived medicines: a novel class of immunological adjuvants. Int Immunopharmacol 11, 390–398.
Li, Q., Wang, W., Zhu, Y., Chen, Y., Zhang, W.J., Yu, P., Mao, G.H., Zhao, T., Feng, W.W., Yang, L.Q., Wu, X.Y., 2017. Structural elucidation and antioxidant activity a novel Se-polysaccharide from Se-enriched Grifola frondosa. Carbohydr. Polym. 161, 42–52.
Ma, P., Liu, H.T., Wei, P., Xu, Q.S., Bai, X.F., Du, Y.G., Yu, C., 2011. Chitosan oligosaccharides inhibit LPS-induced over-expression of IL-6 and TNF-alpha in RAW264.7 macrophage cells through blockade of mitogen-activated protein kinase (MAPK) and PI3K/Akt signaling pathways. Carbohydr. Polym. 84, 1391–1398.
Ma, Y., Xing, Y., Mi, H., Guo, Z., Lu, Y., Xi, T., 2014. Extraction, preliminary characterization and immunostimulatory activity in vitro of a polysaccharide isolated from Strongylocentrotus nudus eggs. Carbohydr. Polym. 111, 576–583.
Manček-Keber, M., Jerala, R., 2015. Postulates for validating TLR4 agonists. Eur. J. Immunol. 45, 356–370.
Nie, S.P., Cui, S.W., Phillips, A.O., Xie, M.Y., Phillips, G.O., Al-Assaf, S., Zhang, X.L., 2011. Elucidation of the structure of a bioactive hydrophilic polysaccharide from Cordyceps sinensis by methylation analysis and NMR spectroscopy. Carbohydr. Polym. 84, 894–899.
Pan, D., Wang, L., Chen, C., Hu, B., Zhou, P., 2015a. Isolation and characterization of a hyperbranched proteoglycan from Ganoderma lucidum for anti-diabetes. Carbohydr. Polym. 117, 106.
Pan, D., Wang, L.Q., Chen, C.H., Hu, B.W., Zhou, P., 2015b. Isolation and characterization of a hyperbranched proteoglycan from Ganoderma Lucidum for anti-diabetes. Carbohydr. Polym. 117, 106–114.
Pau-Roblot, C., Lequart-Pillon, M., Apanga, L., Pilard, S., Courtois, J., Pawlicki-Jullian, N., 2013. Structural features and bioremediation activity of an exopolysaccharide produced by a strain of Enterobacter ludwigii isolated in the Chernobyl exclusion zone. Carbohydr. Polym. 93, 154–162.
Petrovsky, N., Cooper, P.D., 2011. Carbohydrate-based immune adjuvants. Expert Rev. Vaccines 10, 523–537.
Pu, X., Ma, X., Liu, L., Ren, J., Li, H., Li, X., Yu, S., Zhang, W., Fan, W., 2016. Structural characterization and antioxidant activity in vitro of polysaccharides from angelica and astragalus. Carbohydr. Polym. 137, 154.
Shakhmatov, E.G., Belyy, V.A., Makarova, E.N., 2017. Structural characteristics of water-soluble polysaccharides from Norway spruce (Picea abies). Carbohydr. Polym. 175, 699.
Shang, M., Zhang, X., Dong, Q., Yao, J., Liu, Q., Ding, K., 2012. Isolation and structural characterization of the water-extractable polysaccharides from Cassia obtusifolia seeds. Carbohydr. Polym. 90, 827–832.
Sheu, S.C., Ying, L., Lee, M.S., Cheng, J.H., 2013. Immunomodulatory effects of polysaccharides isolated from Hericium erinaceus on dendritic cells. Process Biochem. 48, 1402–1408.
Shi, Y., Zhao, L., Liu, X., Hu, F., Cui, F., Bi, Y., Ma, Y., Feng, S., 2012. Structural characterization of a sulfated glucan isolated from the aqueous extract of *Hedysarum polybotrys* Hand.-Mazz. Carbohydr. Polym. 87, 160–169.
Shu, C., Sankaran, B., Chaton, C., Herr, A., Mishra, A., Peng, J., Li, P., 2013. Structural insights into the functions of TBK1 in innate antimicrobial immunity. Structure 21, 1137.
Sun, H., Zhang, J., Chen, F., Chen, X., Zhou, Z., Wang, H., 2015. Activation of RAW264.7 macrophages by the polysaccharide from the roots of Actinidia erianthа and its molecular mechanisms. Carbohydr. Polym. 121, 388–402.
Takeda, K., Akira, S., 2005. Toll-like receptors in innate immunity. Int. Immunol. 17, 1.
Vallabhapurapu, S., Matsuzawa, A., Zhang, W., Tseng, P.H., Keats, J.J., Wang, H., Vignali, D.A., Bergsagel, P.L., Karin, M., 2008. Nonredundant and complementary functions of TRAF2 and TRAF3 in a ubiquitination cascade that activates NIK-dependent alternative NF-kappaB signaling. Nat. Immunol. 9, 1364.
Wang, W., Zou, Y., Li, Q., Mao, R., Shao, X., Jin, D., Zheng, D., Zhao, T., Zhu, H., Zhang, L., 2016. Immunomodulatory effects of a polysaccharide purified from Lepidium meyenii Walp. on macrophages. Process Biochem. 51, 542–553.

Wang, Y., Wang, Y., Mcneil, B., Harvey, L.M., 2007. Maca: an Andean crop with multi-pharmacological functions. Food Res. Int. 40, 783–792.
Wu, D.T., Xie, J., Wang, L.Y., Ju, Y.J., Lv, G.P., Leong, F., Zhao, J., Li, S.P., 2014. Characterization of bioactive polysaccharides from Cordyceps militaris produced in China using saccharide mapping. J Funct Food 9, 315–323.
Wu, J., Yang, X., Zhang, Y.F., Wang, Y.N., Liu, M., Dong, X.Q., Fan, J.J., Yu, X.Q., 2010. Glucose-based peritoneal dialysis fluids downregulate toll-like receptors and trigger hyporesponsiveness to pathogen-associated molecular patterns in human peritoneal mesothelial cells. Clin Vaccine Immunol Cvi 17, 757–763.
Xia, Y.G., Liang, J., Yang, B.Y., Wang, Q.H., Kuang, H.X., 2015. Structural studies of an arabinan from the stems of Ephedra sinica by methylation analysis and 1D and 2D NMR spectroscopy. Carbohydr. Polym. 121, 449–456.
Xiao, J.H., Xiao, D.M., Chen, D.X., Xiao, Y., Liang, Z.Q., Zhong, J.J., 2012. Polysaccharides from the medicinal mushroom cordyceps taii show antioxidant and immunoenhancing activities in a d-galactose-induced aging mouse model. Evidence-Based Complementray and Alternative Medicine 15. ID 273435.
Xu, X., Gu, Z., Liu, S., Gao, N., He, X., Xin, X., 2015. Purification and characterization of a glucan from Bacillus Calmette Guerin and the antitumor activity of its sulfated derivative. Carbohydr. Polym. 128, 138–146.
Zha, S., Zhao, Q., Chen, J., Wang, L., Zhang, G., Zhang, H., Zhao, B., 2014. Extraction, purification and antioxidant activities of the polysaccharides from maca (Lepidium meyenii). Carbohydr. Polym. 111, 584–587.
Zhang, M., Wang, G., Lai, F., Hui, W., 2016. Structural characterization and immunomodulatory activity of a novel polysaccharide from Lepidium meyenii. J. Agric. Food Chem. 64, 1921.